Structural Description of Pressure-Induced Amorphization in ZrW_2O_8

David A. Keen,[1] Andrew L. Goodwin,[2] Matthew G. Tucker,[1] Martin T. Dove,[2] John S. O. Evans,[3] Wilson A. Crichton,[4] and Michela Brunelli[4]

[1]*ISIS Facility, Rutherford Appleton Laboratory, Chilton, Didcot, Oxon OX11 0QX, United Kingdom*
[2]*Department of Earth Sciences, University of Cambridge, Downing Street, Cambridge CB2 3EQ, United Kingdom*
[3]*Department of Chemistry, University Science Laboratories, South Road, Durham DH1 3LE, United Kingdom*
[4]*ESRF, BP220, F-38043 Grenoble Cedex, France*

(Received 30 January 2007; published 31 May 2007)

ZrW_2O_8 undergoes a high-pressure amorphization transition above 1.5 GPa to a phase which is recoverable to ambient conditions. Reverse Monte Carlo modeling of neutron and x-ray total scattering data from ZrW_2O_8 recovered from ~4 GPa shows that the large increase in density on pressurizing ZrW_2O_8 is accommodated within the structure by increased bonding between the WO_4 tetrahedra. This increases the tungsten coordination; changes to the ZrO_6 octahedral environment are not required. This densified crystal-based model, which contains significant local disorder within a distorted periodic structure, is also in reasonable agreement with x-ray and neutron total scattering data measured *in situ* at high pressure.

DOI: 10.1103/PhysRevLett.98.225501 PACS numbers: 61.43.Er, 61.10.−i, 61.12.−q, 64.70.Pf

Solid state amorphization is a widely studied effect, recently highlighted in the interpretation of the structural process underlying rewritable digital versatile discs [1]. Pressure-induced amorphization (PIA) falls within this field and is typified by the behavior of ZrW_2O_8. Indeed, the mechanism for amorphization in this system is particularly interesting since crystalline ZrW_2O_8 shows isotropic negative thermal expansion (NTE) [2] and NTE and PIA are believed to be theoretically linked [3].

The structure of high-pressure amorphous ZrW_2O_8 has been a subject of debate since amorphouslike results were first observed in x-ray diffraction and Raman data [4]. Interpretations have been based on changes to cation coordination [5] within a context of large low-energy polyhedral rotations and translations. Others have suggested that the amorphous phase is actually a kinetically hindered mixture of ZrO_2 and WO_3 [6] although this has recently been challenged [7,8]. The crystal structure of ambient condition α-ZrW_2O_8 consists of a network of corner-linked ZrO_6 octahedra and WO_4 tetrahedra, with each of the latter having one formally nonbridging W–O bond. The structure has a low density (0.0573 atoms $Å^{-3}$) and is highly flexible. It transforms to the crystalline γ phase above 0.5 GPa [9]. This phase, albeit of lower symmetry, is topologically similar to the α phase and possesses some shorter W–O contacts between neighboring WO_4 tetrahedra leading to increased coordination [10]. The amorphization transition begins in polycrystalline samples around 1.5 GPa and is complete above 3.5 GPa when the low-pressure Bragg peaks are no longer observed [4]. Both of these high-pressure phases can be recovered to ambient conditions.

In this present study, total scattering and atomistic modeling are used to understand the local structure of this amorphous phase. It is shown that the amorphization process itself, the observed density change, and newly measured local structure information, can all be explained in terms of a structural model in which the originally nonbridging O atoms of crystalline α-ZrW_2O_8 now form W–O–W linkages. In doing so the connectivity of O-bridged W and Zr centers assumes a glasslike topology.

A large ($\simeq$1 cm^3) sample of amorphous ZrW_2O_8 was recovered from repeated loadings of pelleted α-ZrW_2O_8 pressurized to ~4 GPa within a large volume Paris Edinburgh cell. Its density (0.0721 atoms $Å^{-3}$) was determined using a helium micropycnometer. Total scattering data from this sample were measured on the GEM neutron diffractometer at ISIS [11] under ambient conditions and normalized using standard procedures [12]. X-ray total scattering data from a small amount of the same sample were measured under the same conditions on ID31 at the ESRF [13] ($\lambda = 0.41276$ Å). In addition, neutron and x-ray data from an amorphous sample at ~3 GPa formed from crystalline ZrW_2O_8 were collected *in situ* within a Paris Edinburgh cell mounted on the Pearl/HiPr diffractometer at ISIS [14] and ID27 at the ESRF [15] ($\lambda = 0.222\,913$ Å), respectively.

A comparison between the neutron weighted real space total radial distribution function, $G^N(r)$ as defined in [16], for the recovered amorphous and crystalline α-ZrW_2O_8 [17] phases is shown in the inset of Fig. 1. Large oscillations in the crystalline data at high r contrast with the almost featureless amorphous data in this region. There are also significant differences in the low-r features. The intensities of the W–O peak at 1.79 Å imply a coordination reduction from 4 (crystal) to 3 (amorphous) at this distance. The Zr–O crystal peak at 2.07 Å is broader and slightly asymmetric in the amorphous phase and the peak has shifted to 2.11 Å with an intensity corresponding to a coordination of 8.6 if it contained only Zr–O bonds. It is

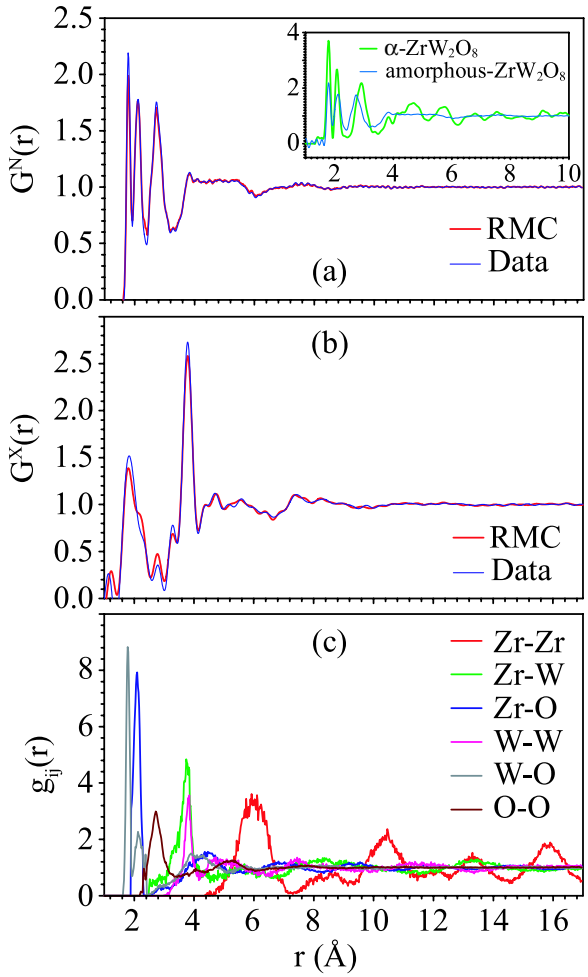

FIG. 1 (color online). (a) Neutron and (b) x-ray weighted pair distribution functions $G(r)$ from recovered amorphous ZrW_2O_8 (thin blue lines) together with the equivalent functions calculated from refined RMC model B (thick red lines). Also shown are the partial pair distribution functions, $g_{ij}(r)$ (c) and a comparison with $G^N(r)$ from crystalline α-ZrW_2O_8 [17] measured at room temperature and pressure (inset).

more likely to contain W–O and Zr–O distances and the intensity is consistent with Zr–O and W–O coordinations of 6 and 2, respectively (although other combinations are possible). The O–O distances around 2.9 Å have shifted to smaller values in the amorphous phase showing that the open network of the crystal has indeed compressed to allow closer O–O contacts both within and between polyhedra. Both $G^N(r)$ and the measured density are incompatible with decomposition to ZrO_2 and WO_3. The volume per formula unit (153 $Å^3$) is larger than the average of a 1:2 mixture of ZrO_2 and WO_3 ($\sim$ 140 $Å^3$ [8]) and the peaks in $G^N(r)$ are in slightly different positions and of different relative intensities to a composite $ZrO_2 + 2WO_3$ $G^N(r)$ [18].

The recovered amorphous phase is 26% more dense than α-ZrW_2O_8. This is a very large change with only 5% accounted for by the α-γ transition [10], but not so large as to consider higher pressure phases such as the 42% more dense α-U_3O_8 structured polymorph with 6 + 1 coordinated Zr and W atoms [8]. This intermediate density must be the result of additional linkages (increased local coordinations) within the network; translations and rotations of the low-pressure structural units alone will not be sufficient. With this in mind there are only two real possibilities (or variations thereon) for the amorphous structure, both based on the α-ZrW_2O_8 crystal topology, and consistent with the expected coordination deduced from $G(r)$ [19].

In both models the nonbridging oxygen atom, O3 (originally bonded only to W2), connects the W1 and W2 atoms; this additional connectivity is present in the structure of γ-ZrW_2O_8 [10]. The difference between the two possible amorphous models lies in the behavior of the remaining nonbridging oxygen atom, O4 (Fig. 2). In the first (model A), concerted translations of the newly formed W_2O_8 unit along the [111] diagonal brings O4 within bonding distance of the nearby Zr atom (originally separated by 3.696 Å). In the second (model B), the W_2O_8 translations are accompanied by small correlated rotations of the polyhedra such that O4 is displaced away from the [111] diagonal towards one of the three nearby W2 atoms (originally at a distance of 3.634 Å). The formation of this second model would likely follow a pattern analogous to the "ice rules" [20] in the sense that for each W_2O_8 unit there are three possible W2 "acceptor sites" and three possible O4 "donor sites, and only one of each can be "filled" with a W1–O4–W2 bond in the amorphous structure. Note that the existence of mechanistic "choice" in this model might encourage amorphization. Model A reflects the findings of earlier lattice dynamical calculations

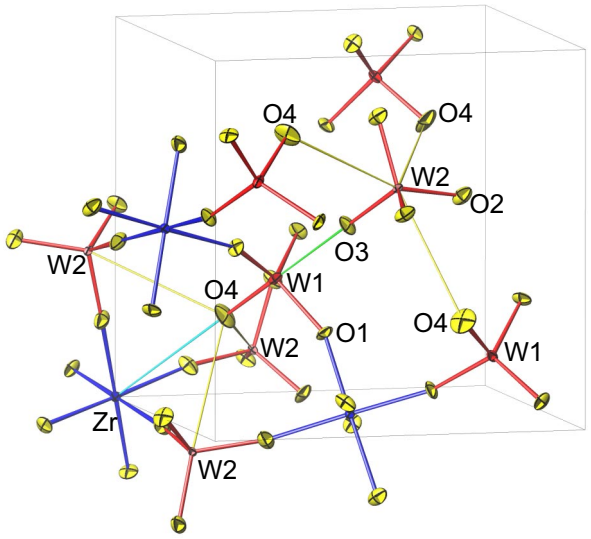

FIG. 2 (color online). A fragment of the α-ZrW_2O_8 crystal structure showing which additional bonds are formed between WO_4 tetrahedra (red) and ZrO_6 octahedra (blue) to create the starting models for the amorphous structure. The green bond (W1 to O3) is formed in all models; the light blue bond (Zr to O4) in model A; a proportion of yellow bonds (W2 to O4) in model B (see text for details). Atom labels refer to [2].

that suggest the formation of additional Zr–O–W linkages under pressure, although implicit symmetry constraints in these calculations would not have allowed an amorphous phase such as model B to emerge [21]. The two models give rise to different coordination numbers: model A gives seven-coordinate Zr atoms and W coordinations of both four (W2) and five (W1); model B retains sixfold coordination of Zr and has five-coordinate W atoms. The O atoms of both models are all twofold coordinated and the bonds in the original crystal structure have been retained.

It is difficult to determine the relative validity of these two models by inspection of the experimental $G(r)$ functions. Consequently, the reverse Monte Carlo (RMC) method as implemented in the program RMCPROFILE [22] was used to refine atomistic configurations, one corresponding to model A and others to different W1–O4–W2 bonding choices corresponding to model B. Starting configurations, each of 2816 atoms, were prepared by establishing an appropriate framework connectivity, and then using the "distance window" constraints within the RMCPROFILE to relax the structure at the required density. In this process, atoms were moved randomly one at a time by small amounts until the distances between all neighboring atoms within the fixed topology were within specified limits: in this case, $1.9 < d_{\mathrm{Zr-O}} < 2.3$ Å, $1.64 < d_{\mathrm{W-O}} < 2.4$ Å, and $2.3 < d_{\mathrm{O-O}} < 3.8$ Å. The models were then further refined using RMCPROFILE against the neutron and x-ray total scattering data ($F^N(Q)$, $G^N(r)$, and $S^X(Q)$; functions as defined in [16]) from the recovered phase, while retaining the distance window constraints.

Each refinement followed an identical RMC minimization. Model B fits the data better than model A with the sum of squared differences between model functions and data all at least 2 times smaller than those from model A. This clearly supports additional W–O–W linkages over additional Zr–O–W. The level of agreement is shown graphically in Figs. 1 and 3. The quality of the fits also suggests that reorganization of the structural topology is not required to fit the data. Although additional randomness may easily be incorporated into model B since the requirement for *exactly* fivefold coordination of W atoms is a further constraint on the choice of additional W–O–W linkages, a model that only required fivefold coordination of W atoms *on average* (e.g., a model closely related to the γ phase) did not improve the fit to the data further.

The partial pair distribution functions, $g_{ij}(r)$, from model B are shown in the bottom panel of Fig. 1. Although $g_{\mathrm{ZrZr}}(r)$ retains oscillations to large distances consistent with a disordered crystal, the $G(r)$ do not. The neutron and x-ray weighting of the $g_{ij}(r)$ functions in the respective $G(r)$ are very different and contribute complementary information; $g_{\mathrm{OO}}(r)$ and $g_{ij}(r)$ involving W dominate $G^N(r)$ and $G^X(r)$, respectively. This is clearly seen in Fig. 1 where there is a strong sharp peak in $G^X(r)$ at the position of the low-r peak in $g_{\mathrm{WW}}(r)$ and only a trough at the position of the low-r peak in $g_{\mathrm{OO}}(r)$; in $G^N(r)$ the

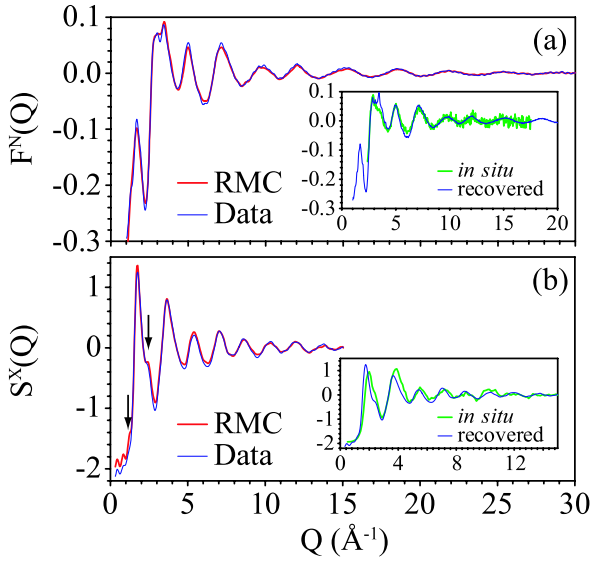

FIG. 3 (color online). (a) Neutron and (b) x-ray structure factor data from recovered amorphous ZrW_2O_8 (thin blue lines) and the equivalent functions obtained from refined RMC model B (thick red lines). The insets show comparisons with data from amorphous ZrW_2O_8 measured at $\simeq 3$ GPa.

situation is reversed with a very small peak and a strong peak at the two positions, respectively. However, in both cases, $g_{\mathrm{ZrZr}}(r)$ has the lowest weighting, and hence these oscillations are not observed in the $G(r)$. It is possible that they can be discerned as very weak peaks in the structure factors, despite their weak overall contribution to these functions. The Zr–Zr partial structure factor peaks strongly at the positions marked by arrows in Fig. 3 and these indeed correspond to very weak features in $S^X(Q)$. The RMC refined model B is shown in Fig. 4. The form of the structure is intriguing: amorphouslike connectivity within a crystal-like Zr array. This demonstrates that so-called "x-ray amorphous" materials can in fact retain some periodicity, particularly if the periodic correlations are weakly weighted in the available data.

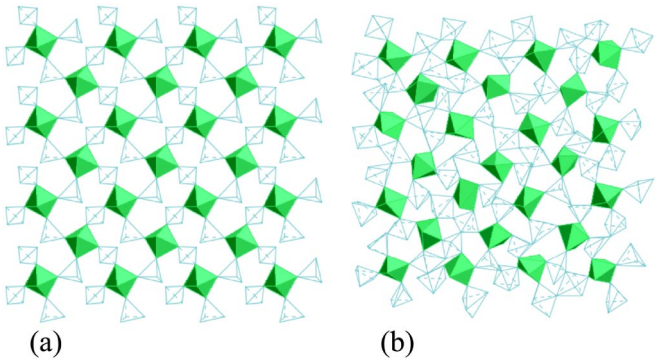

FIG. 4 (color online). Polyhedral representation of a section of (a) α-ZrW_2O_8 and (b) amorphous ZrW_2O_8 from RMC refinement of model B. Green filled and unfilled polyhedra correspond to Zr–O and W–O polyhedra; Zr–O and W–O bonds are defined as atoms less than 2.3 and 2.4 Å apart, respectively.

Figure 3 also shows comparisons between structure factors obtained from recovered amorphous ZrW_2O_8 and those measured *in situ* at high pressure. The structure factors are the same within the error limits of the *in situ* data [23] with the exception of the low-Q peak in $S^X(Q)$ which is shifted to slightly lower Q in the data from the recovered sample. This is probably the result of a density reduction on pressure release and does not necessarily reflect a significant change in the underlying local structure.

The RMC-generated model was constructed via the disordering of a crystal structure through the formation of additional bonds and subsequent relaxation; none of the initial bonds were broken. This is an intuitively attractive process for PIA and it is important to note that such a crystal-based model fits the diffraction data very well. The mechanism is also significantly different from amorphous material formation via melt quenching. Furthermore, the structure makes chemical sense with bond lengths comparable to those of the α phase, and with concerted translations and rotations of polyhedra allowing the structure to fold in on itself, increase its density, and give sensible coordinations. This mechanism is clearly related to the processes involved in NTE of the ambient pressure crystal phases; of the large reciprocal space density of NTE modes in α-ZrW_2O_8 all will soften under pressure by virtue of their negative Grüneisen parameters and many will soften completely at disparate wave vectors resulting in a displacive phase transition to an amorphous phase. The magnitudes of the displacements associated with these condensations are sufficient to bring atoms close enough together to form new bonds. Furthermore, the absence of strain in the structure might explain why the amorphous phase is recoverable to ambient conditions.

It is also worth exploring the relationship between PIA in ZrW_2O_8 and zeolites [24]. In the latter PIA produces both low-density (LDA) and high-density (HDA) amorphous phases which retain and change the crystal topology, respectively. Additional bonds in HDA structures form across the larger aluminosilicate rings to increase density and Si/Al–O coordination. The increased bonding in amorphous ZrW_2O_8 would point to an HDA phase, formed in a similar manner to those of zeolites. However, the irreversible nature of the PIA transition ZrW_2O_8 is different because the amorphous topology of polyhedral units is retained on decompression. In zeolites the Si/AlO_4 tetrahedra are recovered on decompression and irreversible PIA is only observed because a different network topology reforms. The significant difference therefore is the stability of higher coordinated polyhedra in ZrW_2O_8 over those in zeolites at ambient conditions.

In conclusion, a mechanism for PIA in ZrW_2O_8 has been identified that yields an amorphous structure in good agreement with diffraction data. The structure is related to that of the low-pressure crystalline phase and distinct from melt-quenched structures. This mechanism may be generally applicable to other network materials which display amorphization at high pressure.

We acknowledge funding for this work by EPSRC and Trinity College, Cambridge (A. L. G.).

[1] S. Kohara *et al.*, Appl. Phys. Lett. **89**, 201910 (2006).
[2] J. S. O. Evans, W. I. F. David, and A. W. Sleight, Acta Crystallogr. Sect. B **55**, 333 (1999).
[3] R. J. Speedy, J. Phys. Condens. Matter **8**, 10 907 (1996).
[4] C. A. Perottoni and J. A. H. da Jornada, Science **280**, 886 (1998).
[5] T. Varga *et al.*, Phys. Rev. B **72**, 024117 (2005).
[6] A. K. Arora *et al.*, J. Phys. Condens. Matter **16**, 1025 (2004).
[7] C. A. Perottoni, J. E. Zorzi, and J. A. H. da Jornada, Solid State Commun. **134**, 319 (2005).
[8] A. Grzechnik *et al.*, Chem. Mater. **13**, 4255 (2001).
[9] C. Pantea *et al.*, Phys. Rev. B **73**, 214118 (2006).
[10] J. S. O. Evans *et al.*, Science **275**, 61 (1997).
[11] A. C. Hannon Nucl. Instrum. Methods Phys. Res., Sect. A **551**, 88 (2005).
[12] A. C. Hannon, W. S. Howells, and A. K. Soper Inst. Phys. Conf. Ser. **107**, 193 (1990).
[13] A. N. Fitch J. Res. Natl. Inst. Stand. Technol. **109**, 133 (2004).
[14] C. Wilson *et al.*, Rutherford Appleton Laboratory (RAL) Technical Report No. RAL-TR-96-050, 1996, p. 61; RAL Technical Report No. RAL-TR-97-050, 1997, p. 28.
[15] M. Mezouar *et al.*, J. Synchrotron Radiat. **12**, 659 (2005).
[16] D. A. Keen, J. Appl. Crystallogr. **34**, 172 (2001).
[17] M. G. Tucker *et al.*, Phys. Rev. Lett. **95**, 255501 (2005).
[18] This was confirmed by measuring total scattering from separate powdered samples of ZrO_2 and WO_3 on the GEM diffractometer.
[19] The models could equally have been based on the γ-phase structure since it possesses essentially the same topology as the α phase, albeit with some of the tetrahedral pairs in a changed orientation [10]. The impact of the increased disorder within the γ phase on the amorphous structure is slight and beyond the scope of this Letter; it does not impact the general conclusions.
[20] J. D. Bernal and R. H. Fowler, J. Chem. Phys. **1**, 515 (1933).
[21] A. K. A. Pryde, M. T. Dove, and V. Heine, J. Phys. Condens. Matter **10**, 8417 (1998).
[22] M. G. Tucker, D. A. Keen, M. T. Dove, A. L. Goodwin, and Q. Hui, J. Phys. Condens. Matter (to be published).
[23] The geometric constraints of Pearl restrict the Q range over which $F^N(Q)$ can be measured *in situ*, particularly at low Q. Quantitative correction of high-pressure $S(Q)$ data from ID27 is nontrivial; uncertainties in (large) background corrections will only affect peak intensities, not peak positions.
[24] I. Peral and J. Íñiguez, Phys. Rev. Lett. **97**, 225502 (2006); G. N. Greaves *et al.*, Nat. Mater. **2**, 622 (2003).